Two-gap superconductivity seen in penetration-depth measurements of $Lu_2Fe_3Si_5$ single crystals

R. T. Gordon,[1] M. D. Vannette,[1] C. Martin,[1] Y. Nakajima,[2] T. Tamegai,[2] and R. Prozorov[1,*]
[1]*Ames Laboratory and Department of Physics & Astronomy, Iowa State University, Ames, Iowa 50011, USA*
[2]*Department of Applied Physics, The University of Tokyo, Hongo, Bunkyo-ku, Tokyo 113-8656, Japan*
(Received 3 June 2008; revised manuscript received 20 June 2008; published 21 July 2008)

A single crystal of superconducting $Lu_2Fe_3Si_5$ was studied using the tunnel-diode resonator technique in the Meissner and mixed states. The temperature dependence of the superfluid density provides strong evidence for two-gap superconductivity and indicates that there are nearly equal contributions from each gap having magnitudes of $\Delta_1/k_BT_c=1.86$ and $\Delta_2/k_BT_c=0.54$. In the vortex state, the pinning strength shows unusually strong temperature dependence and is nonmonotonic with the magnetic field (peak effect). The irreversibility line is sharply defined and quite distant from the $H_{c2}(T)$ line, which hints at enhanced vortex fluctuations in this two-gap system. Altogether, our findings from electromagnetic measurements provide strong support for the existence of two-gap superconductivity in $Lu_2Fe_3Si_5$, as previously suggested from specific-heat measurements.

DOI: 10.1103/PhysRevB.78.024514 PACS number(s): 74.25.Nf, 74.20.Rp, 74.25.Ha, 74.25.Op

I. INTRODUCTION

Initially, interest in the rare-earth iron containing silicides $M_2Fe_3Si_5$ (M=Y,Sc, and Lu) was due to unusually high superconducting critical temperatures (2.4, 4.5, and 6.0 K, respectively) for compounds containing crystallographically ordered iron sublattices.[1] ^{57}Fe Mössbauer effect measurements indicate that the iron in these materials possess no magnetic moments.[2,3] Further detailed studies have revealed that other superconducting properties are quite unconventional. The upper critical field $H_{c2}(0)$ for $Lu_2Fe_3Si_5$ has been found to be unusually large when compared to the other iron-containing silicide superconductors[4,5] and its temperature dependence differs from convention. Anisotropy and a pronounced peak effect have also been reported in magnetic measurements.[6] The presence of a large residual electronic term in the specific heat below T_c, as well as a reduced specific heat jump at T_c, has been observed and confirmed indicating departure from standard Bardeen-Cooper-Schrieffer (BCS)-like behavior.[7,6] Nonmagnetic impurities have been shown to suppress T_c at a significant rate, which is incompatible with the isotropic *s*-wave BCS picture.[8,9] On the other hand, ac Josephson effect measurements have indicated an *s*-wave pairing mechanism.[10] Vining, Shelton, Braun, and Pelizzone have proposed a two-band model in order to explain their specific-heat data.[7] Their model assumes a two-band Fermi surface with one band being superconducting and gapped, and another being normal. This represents an extreme case of multiband superconductivity as we know it today, for example in MgB_2, where different bands have gaps of different magnitudes.[11,12] Later detailed measurements of $Lu_2Fe_3Si_5$ crystals and analysis have shown that specific-heat data is explained quantitatively well within a two-band model of superconductivity where both bands are gapped but with different gap amplitudes.[13] Recently, a class of superconductors, the iron-containing oxypnictides, was discovered.[14] It has been suggested that these materials could also be multigap superconductors.[15]

In this contribution, precision measurements of the London and Campbell penetration depths are presented, the superfluid density is analyzed, and unusual vortex properties are reported. We conclude that $Lu_2Fe_3Si_5$ is, indeed, a two-gap superconductor. It seems that multiband superconductivity is more widespread and develops when there are different dimensionalities of the Fermi surface on different bands, which leads to reduced interband scattering. In MgB_2 there are two- and three-dimensional bands,[11,12] whereas $Lu_2Fe_3Si_5$ has one- and three-dimensional Fermi surfaces.[13]

II. EXPERIMENT

A. Tunnel-diode resonator technique

Measurements of the $Lu_2Fe_3Si_5$ single crystal were performed using a tunnel diode resonator (TDR).[16–18] An extended review of the use of a TDR to study superconductors is given in Ref. 16. The main components of the TDR are an LC tank circuit and a tunnel diode. The tunnel diode has a region of negative differential resistance in its *I-V* curve. If a dc bias voltage is applied across the diode in this region, then it acts as an ac power source for the LC tank circuit. This results in a self-oscillating circuit, which resonates continuously at a constant frequency for given values of L and *C*. The resonance frequency of the circuit used in our measurements was near 14 MHz. All throughout the measurements the circuit is kept at a constant temperature, 4.8 K $\pm$ 1 mK, allowing for a stability of 0.05 Hz in the resonance frequency over several hours. The sample to be studied is mounted on a sapphire rod with a small amount of Apiezon *N* grease. The sapphire is inserted inside of the inductor coil of the tank circuit. It is important that the sample and its mount do not make physical contact with the coil so that the temperature of the sample may be changed while keeping the circuit at a constant temperature to maintain the stability. As the magnetic susceptibility of the sample changes with temperature, so does the inductance of the tank coil. This results in a change in the TDR resonance frequency. By measuring the shift in the resonance frequency, we are able to sense changes in the penetration depth on the order of 0.5 Angstroms. Specifically, the frequency shift, $\Delta f=f(T)-f_0$, with

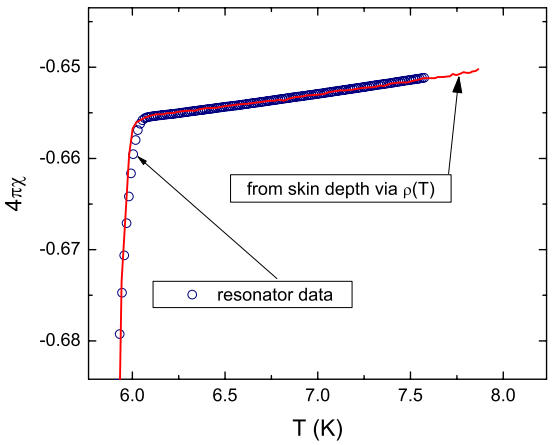

FIG. 1. (Color online) Evaluation of the calibration constant by matching $4\pi\chi(T)$ from the TDR data (circles) to that calculated from the skin depth [solid red curve (dark gray in print)] obtained from the four-point resistivity measurements.

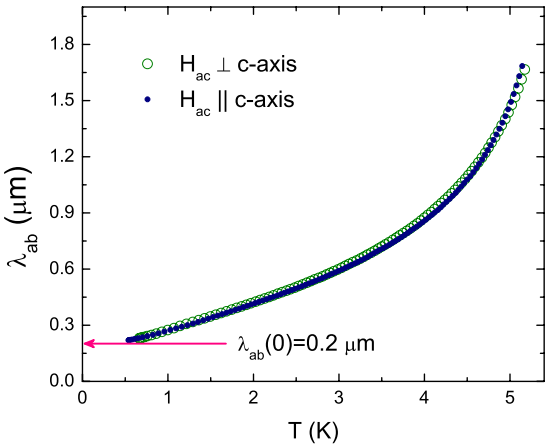

FIG. 2. (Color online) $\lambda_{ab}(T)$ obtained from the measurements in two orientations, see text for details.

respect to the resonant frequency of an empty coil, f_0, is given by

$$\Delta f(T) = -G4\pi\chi(T) = G\left[1 - \frac{\lambda}{R}\tanh\left(\frac{R}{\lambda}\right)\right], \qquad (1)$$

where $G \simeq f_0 V_s / 2V_c(1-N)$ is the geometry-dependent calibration constant, V_s is sample volume, V_c is the effective coil volume, and N is the demagnetization factor. The effective sample dimension R is calculated by using the technique shown in Ref. 17. As described in detail in Ref. 18, it is difficult to obtain the absolute value of the penetration depth due to uncertainties in the sample dimension. However, it is possible to calibrate the system with great accuracy by using the temperature-dependent skin depth, $\delta(T)$, measured just above T_c. In that regime, both the real and imaginary parts of the susceptibility are taken into account and the frequency shift due to the skin effect is $\Delta f(T)_{T>T_c} = G[1 - (\delta/2R)\tanh(2R/\delta)]$. The skin depth, $\delta(T) = c\sqrt{\rho(T)/2\pi\omega}$, is evaluated independently from the temperature-dependent resistivity, $\rho(T)$, measured by the four-probe technique. This is shown in Fig. 1, where resonator data are shown in empty circles and data obtained from measured resistivity are shown as a solid line. Apparently, the agreement is very good. In addition to excellent stability and sensitivity, an advantage of this technique is the use of very low excitation fields, ~20 mOe, which ensures that the sample is in the Meissner state. Furthermore, by superimposing an external dc field, we can probe the vortex state in the so-called Campbell regime, where small excitations ensure that the vortices remain in their potential wells.

B. Samples

The single crystal of $Lu_2Fe_3Si_5$ was grown by the floating-zone technique using an image furnace followed by an annealing as described in detail elsewhere.[13] The sample was a rectangular slab having dimensions $0.99 \times 0.84 \times 0.15$ mm^3 with the c axis perpendicular to the largest face. To study possible anisotropy of the response, the measurements were performed with the excitation field both parallel and perpendicular to the c axis of the sample. A ^{3}He cryostat with the sample in vacuum and applied external fields of up to 9 T was used for the reported studies.

III. RESULTS AND DISCUSSION

A. London penetration depth ($H_{dc}=0$)

Figure 2 shows the temperature dependence of the London penetration depth, $\lambda_{ab}(T)$, obtained from measurements along and perpendicular to the c axis. Both orientations give $\lambda_{ab}(T)$. This is because the penetration depth is proportional to the volume of magnetic field penetrating the sample from different sides. When the excitation field is applied parallel to the c axis, only the in-plane currents circulate and $\lambda_{ab}(T)$ is measured directly. However, this configuration is more difficult to deal with due to a large demagnetization factor. When the excitation field is applied perpendicular to the c axis, currents circulate in both the ab plane and along the c-axis direction. However, since our sample is thin along the c-axis direction, the relative contribution of the currents along this direction, $\sim t/w\lambda_c/\lambda_{ab} \approx 0.16\lambda_c/\lambda_{ab}$, can be neglected and hence $\lambda_{ab}(T)$ is measured for this orientation as well. Here w and t are the planar dimension and thickness, respectively. In addition, the anisotropy of this system is small so the error introduced by the above approximation is minimal. As can be seen in Fig. 2, the penetration depth is very nearly the same for the sample measured in both orientations. The value of $\lambda_{ab}(0)=0.2$ μm was obtained, as described in Ref. 16, from the reversible magnetization $dM/d\ln H$. This was measured independently on the same sample using a *Quantum Design* magnetometer. In further analysis, possible uncertainty in this number up to 25% was examined and confirmed not to change our conclusions in any way.

The symbols in Fig. 3 show the temperature-dependent superfluid density, $\rho_s(T) = [\lambda(0)/\lambda(T)]^2$, calculated from the penetration depth shown in Fig. 2. The solid red curve is the total superfluid density calculated from the α model, which

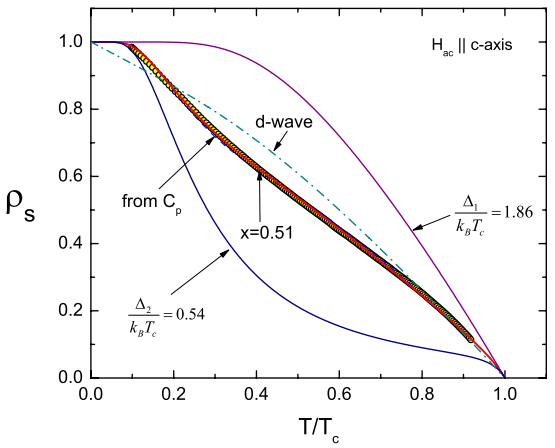

FIG. 3. (Color online) TDR data (symbols) fitted to a two-gap model with indicated parameters. The red curve (dark gray in print) shows the total superfluid density. Also shown and labeled are the two partial superfluid densities as described in the text. The dashed line is calculated from the parameters derived from the specific heat data. The best fit to the *d*-wave order parameter is shown for comparison (dot-dashed line).

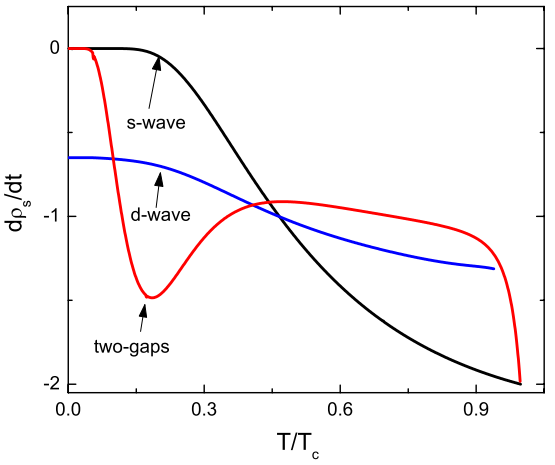

FIG. 4. (Color online) $d\rho_s/dt$ for pure *d*-wave, *s*-wave, and the present case of two-band superconductivity.

assumes two independent contributions to the total superfluid density and has been successfully applied to the well-known two-gap superconductor MgB_2.[11,12] In this model each superconducting gap, denoted by $\Delta_1(T)$ and $\Delta_2(T)$, has a similar temperature dependence as that given by the weak-coupling BCS self-consistency equation.[16] However, there are different ratios of $\Delta_i(0)/k_BT_c$ that become two fitting parameters. A third fitting parameter gives the relative contribution of each band to the total superfluid density, $\rho_{\text{total}}(T)=x\rho_1(T)+(1-x)\rho_2(T)$. Each superfluid density is calculated by using the full temperature range semiclassical BCS treatment as described in detail elsewhere.[16] These partial $\rho_1(T)$ and $\rho_2(T)$ are shown by marked solid lines in Fig. 3. The best fit was achieved with $x=0.51$, $\Delta_1/k_BT_c=1.86$, and $\Delta_2/k_BT_c=0.54$. The first gap is quite close to the weak-coupling value of 1.76, whereas the second gap is much smaller and it is surprising that the earlier two-band model assumed it to be fully normal.[7] Similar to MgB_2, the two gaps contribute equally to the superfluid density. A dashed line, which almost follows the data, is calculated from the parameters obtained from analyzing the specific-heat data. The parameters obtained from this line are $x=0.47$, $\Delta_1/k_BT_c=2.2$, and $\Delta_2/k_BT_c=0.55$.[13] This is in quite good agreement with the values obtained for the superfluid density, given the very different nature of the measurements. To further highlight the qualitative differences between single- and two-gap behavior, we have plotted $d\rho_s/dt$ in Fig. 4. Note the characteristic nonmonotonic behavior in the case of two gaps. It is neither present in the pure *d*-wave nor the pure *s*-wave case.

B. Campbell penetration depth ($H_{\text{dc}}\neq 0$)

While the situation is quite clear for the London penetration depth, measurements in an applied magnetic field reveal more puzzling behavior of the studied compound. When an external dc field is applied and a small amplitude ac response is probed, the vortices respond elastically and the overall susceptibility is governed by the Campbell penetration depth, $\lambda^2=\lambda_L^2+\lambda_C^2$, where λ_L is the usual London penetration depth described above, and $\lambda_C(B,T,j)$ is the Campbell penetration depth,[19] $\lambda_C^2=\phi_0 B/4\pi\alpha(j)$. Here ϕ_0 is the flux quantum and $\alpha(j)$ is the Labusch parameter that generally depends on the biasing Bean current generated in the sample, for example after applying a field after cooling in zero field. The magnetic susceptibility of the sample (and the frequency shift) in the vortex state is still given by Eq. (1), but with a generalized penetration depth.

In conventional type-II superconductors there is no hysteresis for zero-field-cooled (zfc) and field-cooled (fc) curves of the small amplitude ac response. However, in materials where j_c is strongly temperature dependent (e.g., high-T_c cuprates), a large hysteresis is observed.[19] As shown in Ref. 19, a cubic correction to a parabolic potential well for vortex pinning leads to $\alpha(j)=\alpha_0\sqrt{1-j/j_c}$, where $j_c=c\alpha_0 r_p/\phi_0$ is the critical current and r_p is the radius of the pinning potential. This model explains why the zero-field-cooled curve differs from subsequent cooling and warming, and it was successfully used to explain the data for the $Bi_2Sr_2CaCu_2O_{8+y}$ superconductor.

$4\pi\chi(T)$ in the vortex state of $Lu_2Fe_3Si_5$ is shown in Fig. 5 for three representative fields. In each case the sample was cooled in zero applied field to the base temperature and the indicated magnetic field was applied. Then the measurements were taken while warming up the sample above T_c (zfc-w). Then, the sample was cooled and warmed twice without changing the field and while taking the data ($fc-c$ and $fc-w$). For low field values there is no hysteresis observed, while at intermediate fields the hysteresis becomes very pronounced. Clearly, the hysteresis is associated with the static Bean current, j, induced by applying field. We also note that this effect is not associated with the vortex density (e.g., less vortices after zfc) because then the initial Campbell length would be smaller than it is at equilibrium, not larger as observed.

By measuring many $4\pi\chi(T)$ curves at different magnetic fields, we extracted field dependence of the initial suscepti-

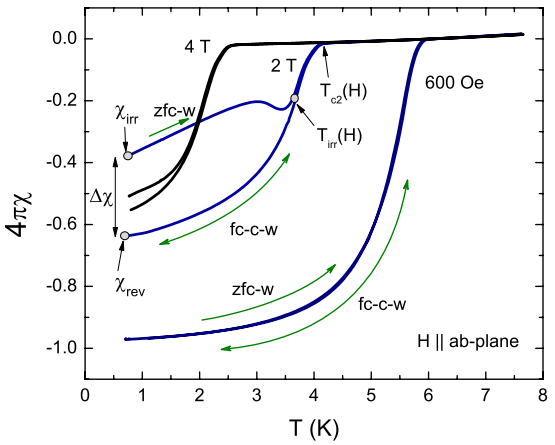

FIG. 5. (Color online) $4\pi\chi(T)$ from the TDR data at three different values of an applied magnetic field along the c axis. Each curve was obtained after cooling in zero field and then warming and cooling twice. The labels and arrows indicate various characteristic points used in later analysis.

bility obtained after zfc and fc. Figure 6 shows the resulting $4\pi\chi_{irr}(H)$ (open circles) and $4\pi\chi_{rev}(H)$ (closed squares) curves at $T=0.7$ K. Figure 7 shows the difference between the two curves. This difference is directly related to the strength of pinning and magnitude of the apparent Bean current density, j, $\Delta\chi \sim j/j_c$, where we have assumed $j \ll j_c$. There is a clear peak effect and its location is quite compatible with direct measurements reported in Ref. 6.

Finally, we construct the $H-T$ phase diagram obtained from our measurements for both directions. While the Meissner response is governed by currents flowing in the *ab* plane, in an applied magnetic field the response is anisotropic and is determined by the orientation of the vortices with respect to the crystal axes. We observe large anisotropy of the upper critical field, $H_{c2}(T)$, down to 1 K as shown in Fig. 8, which has not been reported in earlier papers. Furthermore, $H_{c2}(T)$, determined from the TDR measurements, is in excellent agreement with the specific-heat data. Note that $H_{c2}(T)$ is linear in temperature down to $0.15T_c$. Figure 8 also shows

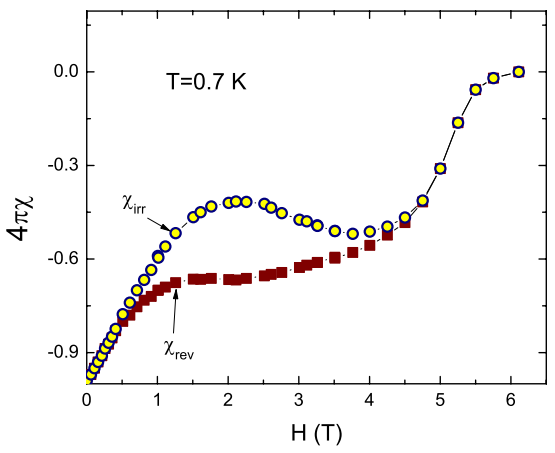

FIG. 6. (Color online) Open circles: $4\pi\chi_{irr}(H)$ at $T=0.7$ K measured by applying field after zfc, as indicated in Fig. 5. Closed squares indicate $4\pi\chi_{rev}(H)$ obtained on fc.

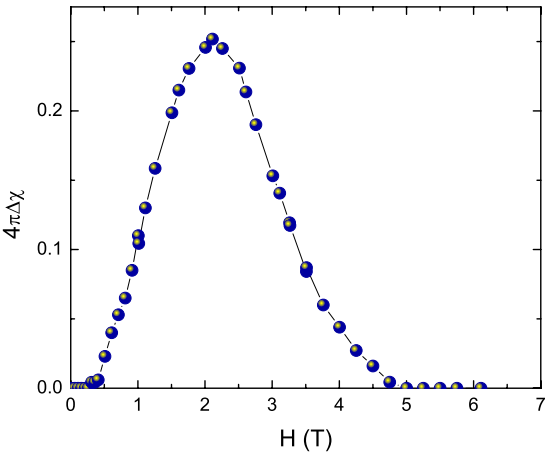

FIG. 7. (Color online) The difference between zfc and fc curves shown in Fig. 6, $4\pi\Delta\chi=4\pi\chi_{irr}-4\pi\chi_{rev}$.

position of the irreversibility line (see Fig. 5 for definition) for both orientations. Unlike conventional superconductors, where $H_{irr}(T)$ is very difficult to determine due to its gradual merging into $H_{c2}(T)$, in $Lu_2Fe_3Si_5$ it is sharply defined and is quite distant from the $H_{c2}(T)$. This is another indication of significant reduction of the critical current possibly due to enhanced fluctuations in the two-gap system.

IV. CONCLUSIONS

In conclusion, we have found that $Lu_2Fe_3Si_5$ shows a Meissner response compatible with two-gap *s*-wave superconductivity. In the vortex state, it shows unusually strong temperature dependence of the critical current, which is also nonmonotonic with magnetic field (peak effect). The upper critical field is anisotropic and linear in temperature. All these observations are reminiscent of unconventional superconductivity and further theoretical insight to connect these properties is needed.

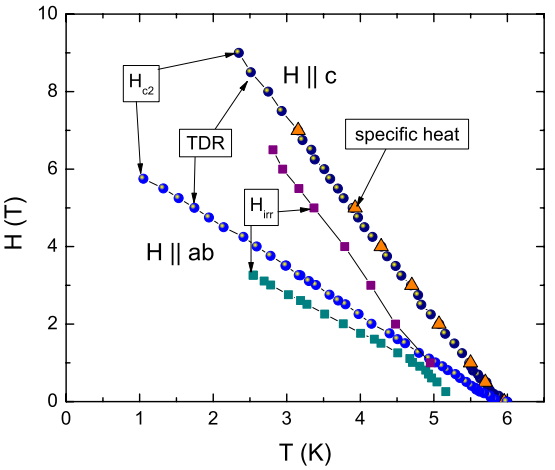

FIG. 8. (Color online) H-T phase diagram for $Lu_2Fe_3Si_5$ crystal in two orientations.

ACKNOWLEDGMENTS

Discussions with P. C. Canfield and V. G. Kogan are greatly appreciated. Work at the Ames Laboratory was supported by the U.S. Department of Energy-Basic Energy Sciences under Contract No. DE-AC02–07CH11358. Work at the University of Tokyo was supported by a Grant-in-Aid for Scientific Research from the Ministry of Education, Culture, Sports, Science and Technology. R.P. acknowledges partial support from NSF Grant No. DMR-05–53285 and the Alfred P. Sloan Foundation.

*Corresponding author: prozorov@ameslab.gov

[1] H. F. Braun, Phys. Lett. **75A**, 386 (1980).
[2] J. D. Cashion, G. K. Shenoy, D. Niarchos, P. J. Viccaro, and C. M. Falco, Phys. Lett. **79A**, 454 (1980).
[3] H. F. Braun, C. U. Segre, F. Acker, M. Rosenberg, S. Dey, and P. Deppe, J. Magn. Magn. Mater. **25**, 117 (1981).
[4] G. R. Stewart, G. P. Meisner, and C. U. Segre, J. Low Temp. Phys. **59**, 237 (1985).
[5] A. M. Umarji, S. K. Malik, and G. K. Shenoy, J. Appl. Phys. **57**, 3118 (1985).
[6] T. Tamegai, T. Nakagawa, and M. Tokunaga, Physica C **460-462**, 708 (2007).
[7] C. B. Vining, R. N. Shelton, H. F. Braun, and M. Pelizzone, Phys. Rev. B **27**, 2800 (1983).
[8] H. F. Braun and C. U. Segre, Bull. Am. Phys. Soc. **26**, 343 (1981).
[9] T. Xu and R. N. Shelton, Solid State Commun. **68**, 395 (1988).
[10] R. J. Noer, T. P. Chen, and E. L. Wolf, Phys. Rev. B **31**, 647 (1985).
[11] F. Bouquet, Y. Wang, R. A. Fisher, D. G. Hinks, J. D. Jorgensen, A. Junod, and N. E. Phillips, Europhys. Lett. **56**, 856 (2001).
[12] F. Manzano, A. Carrington, N. E. Hussey, S. Lee, A. Yamamoto, and S. Tajima, Phys. Rev. Lett. **88**, 047002 (2002).
[13] Y. Nakajima, T. Nakagawa, T. Tamegai, and H. Harima, Phys. Rev. Lett. **100**, 157001 (2008).
[14] Y. Kamihara, T. Watanabe, M. Hirano, and H. Hosono, J. Am. Chem. Soc. **130**, 3296 (2008).
[15] V. Barzykin and L. P. Gorkov, arXiv:0806.1933 (unpublished).
[16] R. Prozorov and R. W. Giannetta, Supercond. Sci. Technol. **19**, R41 (2006).
[17] R. Prozorov, R. W. Giannetta, A. Carrington, and F. M. Araujo-Moreira, Phys. Rev. B **62**, 115 (2000).
[18] R. Prozorov, R. W. Giannetta, A. Carrington, P. Fournier, R. L. Greene, P. Guptasarma, D. G. Hinks, and A. R. Banks, Appl. Phys. Lett. **77**, 4202 (2000).
[19] R. Prozorov, R. W. Giannetta, N. Kameda, T. Tamegai, J. A. Schlueter, and P. Fournier, Phys. Rev. B **67**, 184501 (2003).